

# RECENT SEISMICITY AND CRUSTAL STRESS FIELD IN THE LUCANIAN APENNINES AND SURROUNDING AREAS (SOUTHERN ITALY): SEISMOTECTONIC IMPLICATIONS

C. Maggi\*(1,2), A. Frepoli(1), G. B. Cimini (1), R. Console (1,2), M. Chiappini (1)

1. Istituto Nazionale di Geofisica e Vulcanologia (INGV), via di Vigna Murata, 605, 00143, Rome, Italy.

2. Centro di Geomorfologia Integrata per l'Area del Mediterraneo (CGIAM), Potenza, Italy.

\*Corresponding author. Fax: +39-06-51860397

E-mail address : [maggi@ingv.it](mailto:maggi@ingv.it) (C. Maggi).

## Abstract

We analyzed the instrumental seismicity of Southern Italy in the area including the Lucanian Apennines and Bradano foredeep, making use of the most recent seismological data base available so far. P- and S-wave arrival times, recorded by the Italian National Seismic Network (RSNC) operated by the Istituto Nazionale di Geofisica e Vulcanologia (INGV), were re-picked along with those of the SAPTEX temporary array deployed in the region in the period 2001-2004. For some events located in the upper Val d'Agri, we also used data from the Eni-Agip seismic network. We examined the seismicity occurred during the period between 2001 and 2006, considering events with magnitudes  $M \geq 2.0$ . Firstly, we computed the  $V_P/V_S$  ratio using a modified Wadati method, obtaining a value of 1.83. Secondly, through the use of the VELEST code, we carried out an analysis for the one-dimensional (1D) velocity model that approximates the seismic structure of the study area. Third, we relocated the earthquakes and, for well recorded events, we also computed 108 fault plane solutions. Finally, from this focal mechanism dataset we selected 65 solutions, the more constrained, and used them in an inversion procedure for regional stress information.

Earthquake distribution shows three main seismic regions: the westernmost (Apenninic chain) characterized by high background seismicity, mostly with shallow hypocenters, the easternmost below the Bradano foredeep and the Murge with deeper and more scattered seismicity, and finally the more isolated and sparse seismicity localized in the Sila Range and in the offshore area along the Northeastern Calabrian coast. Focal mechanisms computed in this work are in large part normal and strike-slip solutions and their tensional axes (*T*-axes) have a generalized NE-SW orientation. The denser station coverage allow us to obtain improved hypocenters compared to those obtained by using only RSNC data, observing a well relocated and already known presence of sub-crustal seismicity in the study area.

**Key words:** Lucanian Apennines, Southern Italy, seismicity, 1D velocity model, focal mechanisms, stress field.

## 1. Introduction

The Southern Apennines belong to the complex geodynamic setting characterizing the Central Mediterranean region, which is dominated by the NNW-SSE convergence between the European and African plates (*Argus et al.*, 1989; *De Mets et al.*, 1990). The tectonics of this area is accommodated by the collision between the Adriatic microplate and the Apenninic belt. The eastward migration of the extension-compression system derived by the subduction process of the Adriatic microplate is related to the opening of the Tyrrhenian basin (*Barberi et al.*, 2004). Seismological studies and recent geodetic observations reveal that the Apennines are undergoing a NE-trending extension, with seismic deformation rates higher in the southern portion (*Di Luccio et al.*, 2005).

Highly energetic events in the last four centuries are historically well documented. The strongest events are localized in the Apenninic chain as, e.g., the 1694 earthquake that hit the Irpinia-Basilicata area with effects of the XI degree on the Mercalli-Cancani-Sieberg (MCS) scale and the 1857 Basilicata earthquake, located in the upper Val d'Agri and Vallo di Diano, with effects of the XI degree MCS. The latest strong earthquake hit the Irpinia-Basilicata area in 1980 with effects of the X degree MCS and normal mechanism of rupture (*Boschi et al.*, 1990). On the contrary, the foredeep and foreland areas to

the South of the Ofanto river do not show considerable historical earthquakes with the exception of the 1560 event that hit the towns of Barletta and Bisceglie with effects of the VIII degree MCS.

From the instrumental seismic catalogue 1981-2002 (*Castello et al.*, 2005) we observe that most of the background seismicity is concentrated along the Apenninic chain (Fig.1). Three main clusters of earthquakes are observable. The first, in the Potentino area, where concentrated the earthquakes of the two seismic sequences occurred in the years 1990 (*Azzara et al.*, 1993; *Ekström*, 1994) and 1991 (*Ekström*, 1994), both produced by E-W oriented strike-slip structures, and the second, in the Irpinia region. Finally, the last cluster in the Castelluccio area (1998 seismic sequence) with pure normal focal mechanism, close to the northwestern border of the Pollino range (*Michetti et al.*, 2000; *Pondrelli et al.*, 2002). The seismicity in the area between the Vallo di Diano and the upper Val d'Agri is sparse as in the external areas of the Bradano foredeep and the Apulia foreland.

The area of the Lucanian Apennines is one of the main seismically active region of southern Italy, and for this reason is important to improve our knowledge about its crustal and subcrustal structures. The main goal of this paper is providing new insights on the seismotectonic in this portion of the Apenninic chain through a careful analysis of both the hypocentral distribution of background seismicity and active stress field information retrieved from fault plane solution inversion. Present-day stress field data are important for the seismotectonic zonation, a basic tool for seismic hazard evaluation, and are helpful to predict the behaviour of seismogenic faults. Taking advantage of the availability of a denser coverage of seismic stations in the area, we created a high-quality database of local earthquake waveforms recorded during 2001-2006 by the RSNC, the SAPTEX temporary array (2001-2004) (*Cimini et al.*, 2006), and the local ENI-AGIP network in the upper Val d'Agri (Fig.2). This work is subdivided into four steps: (1)  $V_p/V_s$  ratio computation using a modified Wadati method, (2) application of the VELEST code (*Kissling et al.*, 1995) to find the best one-dimensional (1D) velocity model for the study area, (3) relocation of the well-recorded events with the HYPOELLYPSE code (*Lahr*, 1989) to obtain a detailed seismicity distribution of earthquakes; (4) focal mechanisms and regional stress field computation.

## **2. Data selection and $V_p/V_s$ ratio computation**

We re-picked arrival times of earthquakes recorded by the RSNC seismic network and picked those recorded by the temporary SAPTEX network in the period between June 2001 and December 2006. The ENI-AGIP network data were used only for some events located in the upper Val d'Agri and surrounding areas. During the observation period, the permanent network RSNC improved significantly in southern Italy, increasing both the station coverage and the number of three-component extended band (Lennartz 5s) or broad band (Trillum 40s) sensors, which replaced the Kinemtrics S-13 short period sensors. The ENI-AGIP stations are all equipped with three-component Lennartz Lite 1s sensors. Both RSNC and ENI-AGIP networks recode in trigger mode. The SAPTEX stations were equipped with three-component Lennartz 5s sensors and the recording was set in continuous mode for tomographic analysis purpose (*Frepoli et al.*, 2005; *Cimini et al.*, 2006). The database we created is made up by 7570 P- and 4956 S-phases associated to 514 earthquakes with local magnitude  $M_L \geq 2.0$ . Only few events included in this database, and relocated with a quite high number of stations, have  $M_L < 2.0$  (see Table V). We assigned a weight to each P or S arrival on the basis of picking accuracy (see Table I).

To improve the hypocentral depth determination, an average  $V_P/V_S$  ratio is calculated using a modified Wadati method (*Chatelain*, 1978) below shortly described.

If we consider an event  $k$  that is recorded by two stations  $(i,j)$  at hypocentral distances  $x_i$  and  $x_j$ , the time difference between phases  $P_i - P_j$  and  $S_i - S_j$  can be expressed as:

$$DT_P = P_i - P_j = (x_i - x_j)/V_P \quad (1) \quad \text{and} \quad DT_S = S_i - S_j = (x_i - x_j)/V_S \quad (2)$$

where  $V_P$  and  $V_S$  are the P- and S-wave velocity values, respectively. Dividing (2) by (1) we obtain:

$$\frac{DT_S}{DT_P} = \frac{V_P}{V_S} \quad (3)$$

Fitting  $DT_S$  versus  $DT_P$  for all available pairs of stations gives the value of the slope  $V_P/V_S$ . We selected  $DT_S / DT_P$  according to the method used by Pointoise and Monfret (2004). From our data we obtain a  $V_P/V_S$  ratio of 1.83 with 95% prediction bounds, root mean square error (RMSE) of 0.40, and linear correlation coefficient (R) of 0.87 (Fig.3). This value is quite similar to that obtained by other studies in the same region ( $V_P/V_S = 1.82$ , *Frepoli et al.*, 2005).

### 3. Minimum 1D velocity model

In order to better constrain the hypocentral locations we performed an analysis for the best P-wave one-dimensional (1D) velocity model of the study area, using the VELEST algorithm (*Kissling et al.*, 1995). We had to search a simple and laterally homogenous velocity model and station corrections to relocate earthquakes with HYPOELLIPSE. The approach to this problem is finding a 1D model that minimizes the least square solution to the coupled hypocentral-velocity model parameter solution. Since VELEST doesn't invert for changes in layer thickness, we re-stratified the initial model finding a more appropriate model layering. In this way we introduced some layers with thickness of 3 or 4 km, up to 30 km depth, and of 5 km for greater depths. Considering the station elevations, we include an additional layer for all three models with a thickness of 2 km upon the sea level with  $V_p=5$  km/s.

We used three different starting models: the first two were taken directly from the seismological literature as *Chiarabba and Frepoli (1997)* and *Chiarabba et al. (2005)*, respectively. The last is obtained using data of some Lucanian Apennine seismic studies. We selected all the events with a  $RMS < 1s$ . Because reading errors of long-travelling phases can be large, we used only the direct P-wave arrivals, i.e. the stations with a maximum epicentral distance around 150 km. In fact, the  $P_n$  arrival times might create problems in the events re-location and in the computation of the 1D velocity model. Moreover, we considered all the earthquakes located with a station distribution characterized by an average seismic gap  $=145^\circ$ .

#### 3.1. First model

The first starting model was computed for Southern Italy by Chiarabba and Frepoli, 1997, and it is composed by seven layers with a linear increase of velocity with depth. The re-stratified model is called *Modell1*. We perform inversions with VELEST many times to reduce the number of layers: adjacent layers with similar velocity are merged together. In this way, using the best 370 events of our dataset, we computed the 1D velocity model *Vel\_9* (Fig.4) with an average RMS equal to 0.35s. This model shows a Moho at 26 km depth. Figure 5 shows a large concentration of earthquakes in the depth interval 12-23

km, while at greater depth intervals the smaller amount of events doesn't allow us to improve the velocity model within the deeper layers.

### 3.2. *Second model*

The second starting model is a regional model computed by *Chiarabba et al.* (2005) for the Italian region. It is characterized by seven layers and by a velocity inversion at 20 km of depth, within the lower crust beneath the belt. We re-stratified the initial model (*Model2*) and repeated the VELEST procedure more times to reduce the number of layers obtaining the final model *Vel\_8* (Fig.6). In this inversion we used the best 368 selected events. The final model shows a Moho at 29 km depth and the average RMS is equal to 0.33s. With this model we have a greater density of earthquake hypocenters within the 3-20 km depth interval (Fig.7).

### 3.3. *Third model*

The third starting model, called *Test*, is obtained from some Lucanian Apennines seismic studies (*Barberi et al.*, 2004; *Cassinis et al.*, 2003; *Merlini et al.*, 2001; *Tiberti et al.*, 2005). It is composed by six layers with a linear increase of velocity with depth. The correspondent re-stratified model is called *Teststra*. With VELEST we reduce adjacent layers having the same velocity and computed the final model *Test8* (Fig.8) using the 368 selected events. The Moho is at 35 km depth and the final RMS is 0.33s. Figure 9 shows a strong concentration of earthquake hypocentres within a 5-17 km depth range.

### 3.4. *Model comparison*

As shown in Fig.10, the three final models converge mainly in the upper layers where there is a larger density of earthquakes. This is especially evident for models *Vel\_8* and *Test8*. Moreover, in models *Vel\_8* and *Test8* there are no velocity changes within the most shallow layer at 0 km. The Moho in the final model *Vel\_9* is located at 26 km depth. This is in disagreement with the geological setting of the crust in this region, well-known from seismic exploration method of wide angle reflection-refraction (DSS), gravity anomaly and seismic studies (*Cassinis et al.*, 2003; *Merlini et al.*, 2001; *Tiberti et al.*, 2005). In this area the Moho is found around 30-35 km and is characterized by a doubling of Moho itself. In fact, its depth increases from 15-25 km moving from the Tyrrhenian Sea to the chain axis

(Tyrrenian Moho), and reaches 30-35 km in the foreland (Adriatic Moho) (*Ventura et al.*, 2007). Therefore, we used both models (*Vel\_8* and *Test8*) for localization, with a Moho at 29 and 35 km of depth, respectively.

#### 4. Earthquakes relocation

We relocated the starting dataset of 514 events with the HYPOELLIPSE code using the two models named *Vel\_8* and *Test8*. We take into account earthquakes with azimuthal gap  $< 180^\circ$  and root mean square of the travel-time residuals  $RMS < 1.0$  s. This value is obtained through the equation:

$$RMS = \left[ \frac{\sum_i^n W_i R_i^2}{\sum_i^n W_i} \right]^{\frac{1}{2}} \quad i = 1, \dots, n \quad (4)$$

where  $R_i$  is the residual of the  $i^{th}$  phase and  $W_i$  is the computed weight of the  $i^{th}$  phase. In this way we re-localized 304 events using model *Vel\_8*, with an average  $RMS=0.30$ s and 359 earthquakes using model *Test8*, with an average  $RMS=0.37$ s. Considering model *Vel\_8* we have 56,9% of events with quality A and 23,10% quality B. Whereas considering the second model (*Test8*) we have 67,7% of earthquakes with quality A and 16,4% events quality B (see Table II). From these results it is clear that model *Test8* (Table III) is the best velocity model for the study area.

Using a denser station coverage, in comparison with that available in the past years, we obtained a significant improvement in the hypocentral locations and a well-defined seismicity distribution outlining the main tectonic features of this area. Analyzing the hypocentral distribution obtained using the velocity model *Test8* (Fig.11 and 12), we observe that most of earthquakes are localized beneath the Apenninic chain. The seismicity distribution shows three main seismic zones. The westernmost, of these is characterized by an earthquake distribution centred mainly along the axis of the Lucanian Apennine with maximum hypocentral depths up to 20 km (see Fig.12, section AB, CD, EF and GH). Only few subcrustal events are present within this crustal domain. The second seismic zone is defined by a sparse and deeper seismicity (see Fig.12) localized within the eastern and outer margin of the chain and in the foredeep with depths down to 30 km. The last zone (see Fig.12, section IL and MN) is localized within

the Sila Range also characterized by a sparse seismicity and maximum hypocentral depths around 30 km. Considering section MN in Figure 12, the seismicity reaches 40 km beneath the Southern Apennines with an increase of hypocentral depth in the middle portion of the section, beneath the Lucanian region. This section shows three clusters of hypocentres: the first is located in the Irpinia area, the second is close to the Potentino area and the last beneath the Moliterno area (Val d'Agri). Moreover, through the view of this section we observe clearly a seismic gap between the Pollino and the Sila Ranges. An isolated 88 km deep event is located within the Southern Tyrrhenian subduction zone, beneath the Castelluccio area. This earthquake belongs to the sparse seismicity that characterizes the northern edge of the subduction zone. Figure 13 shows the error ellipses with the 99% confidence limits of the relocated earthquakes. Events with D quality are excluded from this figure (see TableII). Error ellipses show the good quality of the epicentral re-locations. From figure 14 we observe that the results of the relocation are characterized by a large number of events with RMS of 0.2-0.3 s, maximum horizontal errors (Max\_Err\_H) between 0.12-1.2 km and vertical errors (Err\_Z) less than 1 km. All these results outline the high quality of our database.

## **5. Focal mechanisms and stress tensor inversion**

### *5.1 Focal mechanism computation*

We computed 108 first-motion focal mechanisms with at least eight clear observations using the FPFIT code (*Reasenberg and Oppenheimer, 1985*). From this dataset we selected 65 fault plane solutions following the two output quality factors  $Q_f$  and  $Q_p$  ranging from A to C for decreasing quality (Table IV).  $Q_f$  gives information about the solution misfit of the polarity data  $F_j$ , while  $Q_p$  reflects the solution uniqueness in term of 90% confidence region on strike, dip and rake. The selected focal mechanisms for which A-A ( $Q_f$ - $Q_p$ ), A-B, B-A and B-B quality are obtained, are relatively well constrained (Table V, Fig.15a and b). Focal mechanisms with quality A-A are 34, those with A-B and B-A are 27, and those with B-B are 4 (Table V). All fault-plane solutions with quality C for one of the two quality factors are rejected. The average number of polarities for event used in this study is 12. As shown from focal mechanisms of larger events, also from fault plane solutions of background seismicity we observe a



widespread NE-SW extension in the Lucanian Apennine. Focal mechanisms calculated in this work are in large part normal and strike-slip solutions and their tensional axes (*T*-axes) have a generalized NE-SW orientation.

### *5.2 Stress tensor inversion*

We applied the Gephart and Forsyth (1984) procedure, which was further implemented by Gephart (1990), to invert the focal mechanisms for the principal stress axes ( $\sigma_1$ ,  $\sigma_2$ ,  $\sigma_3$ ) and the parameter *R*, which is a relative measure of stress magnitude defined as  $(\sigma_2 - \sigma_1)/(\sigma_3 - \sigma_1)$ . The inverse method using focal mechanism data cannot determine the absolute magnitude of the deviatoric and isotropic stresses. It only can identify the best stress tensor model that most closely matches all the fault plane solutions of the source region. The method requires the basic assumptions that the stress is uniform in space and time in the investigated volume. The brittle shallow crust generally includes small pre-existing faults of any orientation that may have low frictional coefficients. Earthquakes are shear dislocations on these pre-existing faults and slip occurs in the direction of the resolved shear stress on the fault plane. There is mechanical consistency between the slip direction and the principal stress axes,  $\sigma_1$  and  $\sigma_3$ , when these are oriented somewhere within the dilatational and compressional quadrants of the double-couple seismic radiation pattern.

Discrepancy between stress tensor orientation and an observation is defined by a misfit measure which is given by the angular difference between the observed slip direction on a fault plane and the shear stress on that fault plane derived from a given stress tensor. Misfit is computed through an angular rotation about an axis for both nodal planes of each focal mechanism on a grid search of stress tensors. The stress tensor orientation that provides the average minimum misfit is assumed to be the best stress tensor for a given population of focal mechanisms.

We excluded from the inversion procedure 13 focal mechanisms, out of the 65 best selected fault plane solutions, which do not belong to the clustered seismicity located within the Apenninic chain. This allows us to define the boundary of smaller crustal volumes approaching better the assumption of the uniform spatial stress field. We performed a first inversion with 51 focal mechanisms, all located inside

the Apenninic chain from the Pollino Range to the Northern Irpinia area. The minimum average misfit is 7.9, corresponding to a stress tensor with a sub-horizontal  $\sigma_3$  (plunge  $1^\circ$ ) NE-SW directed, an NW-SE sub-horizontal  $\sigma_2$  and a sub-vertical  $\sigma_1$  (plunge  $82^\circ$ ) (Fig.14a). The 95% confidence intervals of the principal stress axes do not overlap, suggesting that the three axes are well constrained by the data. The stress ratio near the solution is between 0.5 and 0.6, constraining the three principal stress axes to be well separated in their absolute values. Notwithstanding the good results in agreement with previous studies showing the general extension in a NE-SW direction of this part of the Apenninic chain, misfits larger than 6.0 suggest an inhomogeneous stress distribution within the considered crustal volume (Wyss *et al.*, 1992).

For this reason we performed two new inversions dividing the dataset into two sub-volumes (see Fig.15a and 15b): one to the North, including the Irpinia and Potentino areas with 32 focal mechanisms, and the other to the South, including the Moliterno and the North-western Pollino Range with 19 fault-plane solutions. The Irpinia-Potentino inversion results show a stress tensor with an orientation very similar to that obtained by the whole dataset (Fig.16b). The factor shape parameter R is between 0.4 and 0.5, while the misfit is quite large (7.4). On the contrary, the misfit that we get from the Moliterno-North-western Pollino Range inversion is smaller than 6.0 (5.1), suggesting a more homogenous stress field in this area. The minimum stress axes ( $\sigma_3$ ) is sub-horizontal and NE-SW oriented and  $\sigma_1$  is quite close to the vertical ( $64^\circ$  plunge) (Fig.16c).

We try to work out the stress tensor heterogeneity inside the Northern sector sub-dividing it further in two portions on the basis of a recent zonation map (Meletti *et al.*, 2004). In particular, we delimited an eastern area called Potentino, including 15 events, and a western area relating to Irpinia, including 14 fault-plane solutions. This subdivision follows the eastward deepening of the hypocentral depths from the inner to the outer margin of the belt. The Potentino area, within which are located the 1990 and 1991 seismic sequences, both characterized by mainshocks with strike-slip focal mechanisms (Azzara *et al.*, 1993; Ekström, 1994), shows an inversion result with an almost oblique stress tensor ( $\sigma_1$  and  $\sigma_2$  with plunge  $58^\circ$  and  $25^\circ$ , respectively) and with a  $\sigma_3$  sub-horizontal and NNE-directed (Fig.16e). This stress

tensor orientation, together with the R parameter value of 0.3, points out a stress field half-way between a pure extensional and a pure strike-slip regime. On the other way, the inversion result of the Irpinia area shows an almost pure stress extensional regime with a sub-horizontal and NE-directed minimum stress axis ( $\sigma_3$ ) (Fig.16d). Moreover, the average misfit (5.9) shows that the stress heterogeneities inside the Irpinia crustal volume are negligible.

## **6. Discussion and conclusions**

The large number of stations available in the last years through the significant improvement of the RSNC coverage and the deployment of the SAPTEX temporary array, allow us to obtain more constrained locations of low magnitude events in the Lucanian region compared to previous studies. We computed the  $V_p/V_s$  ratio, one-dimensional velocity model and station corrections valid for this region to improve the location of the background seismicity. The presence of highly fractured zones related to the main faulting pattern in the study area (*Gentile et al.*, 2000) could determine the relatively high value of the  $V_p/V_s$  ratio we found.

We computed a simple 1D velocity model that fits well the crustal structures of this area. The regional gravity anomaly maps and DSS study outlined the existence of a doubling of the Moho beneath the Southern Apennines (*Morelli*, 2000; *Tiberti et al.*, 2005). This area is characterized by a gravity low, while the two surrounding areas have a gravity high attributed to the overlap of Tyrrhenian and Adriatic Moho (*Tiberti et al.*, 2005). Looking upon these results we obtained a model in which the average Moho is set at 35 km depth, in agreement with the depth estimated for the Italian Peninsula (*Cassinis et al.*, 2003; *Locardi et al.*, 1988).

Most of the seismicity occurred in the area under investigation during the period 2001-2006 is concentrated beneath the Apenninic chain within a  $\sim 350 \times 160$  km NW-SE elongated region. Despite the short time interval of observation, the seismicity examined in this work is representative of the seismic behavior of the Lucanian region as known from longer period of data collection (*Castello et al.*, 2005). In fact, the spatial distribution of the analyzed events closely follows the pattern delineated by the seismicity of the last two decades (Fig.1).

In particular we find that the seismicity is clustered in the Potentino and Irpinia area to the north, and in the Moliterno and northern-western Pollino Range to the south. This distribution enhances a seismic gap located in the Vallo di Diano and Upper Val d'Agri area characterized by very low and sparse background seismicity. Following the macroseismic data and the most recent geological and geomorphological studies (*Maschio et al.*, 2005), within this area, is located the seismogenic structure related to the 1857 Basilicata earthquake (XI MCS). The eastern margin of the chain and the Bradano foredeep are characterized by a more sparse seismicity which shows larger hypocentral depths (generally between 20 and 30 km) than those observed in the inner portion of the chain (generally between 5 and 20 km).

This eastward deepening of the hypocentral depths, from the inner to the outer margin of the belt, indicates a deeper boundary between the brittle and ductile crust beneath the external margin of the Lucanian Apennine and the foredeep, compared to that beneath the chain itself. This increasing seismogenic layer depth is associated with the flexural bending to the West of the Adriatic continental lithosphere beneath the Apenninic chain (*Chiarabba et al.*, 2005). Tomographic and geothermal gradient studies point out a brittle-ductile limit at 28-30 km beneath the foredeep and foreland compared with the 15-18 km of depth of the same limit beneath the chain (*Chiarabba and Amato*, 1996; *Harabaglia et al.*, 1997). These data, together with positive Bouger anomalies, are consistent with the presence of asthenospheric material in the upper mantle below the Tyrrhenian margin of the chain and the adjacent Tyrrhenian Sea (*Scrocca et al.*, 2005).

Few events beneath the Apenninic chain and the Bradano foredeep exhibit depths larger than 30 km. The deepest event is located at ~ 47 km depth beneath the area of Policoro-Montalbano Jonico. This sparse sub-crustal seismicity could be explained as a result of the retreat of the subducting Adriatic lithosphere (*Malinverno & Ryan*, 1986, *Amato et al.*, 1993) as shown in the Northern Apenninic chain, but with the not negligible difference that the Southern Apennines do not show in their external zones an active compression. Moreover, this sub-crustal seismicity is not so evident as that beneath the Northern

Apennines which reaches about 100 km depth. More details on this sub-crustal seismicity will be added with further studies.

We analyzed also the seismicity South of the Pollino Range and the Bradano foredeep. In this area the background seismicity is concentrated in the Sila Range and in the offshore sector of the Ionian Sea, close to the northeastern Calabrian coast (Taranto Gulf). The Castrovillari (Southern Pollino Range) and Piana di Sibari areas appear characterized by lack of the seismicity.

The distribution of focal mechanisms of the background seismicity is helpful in delineating the main seismotectonic provinces of the study region. Our results point to an active extensional regime in this part of the Apenninic chain. Fault-plane solutions computed in this work show tensional axes ( $T$ -axes) generally NE-SW oriented. This widespread NE-SW extension is consistent with previous studies with focal mechanisms of low to moderate magnitude events (*Frepoli and Amato, 2000; Frepoli et al., 2005*), with fault-plane solutions of larger earthquakes (*Pondrelli et al., 2002*) and with breakout analyses (*Cucci et al., 2004; Montone et al., 2004*). It is well-known that the breakout method samples a depth interval between 3 and 6 km, suggesting a continuity in the stress regime at different depths.

A detailed knowledge of the active stress field is necessary in order to constrain the active tectonic processes and the recent geodynamic evolution of the Southern Italian region. The inversion performed with the largest fault-plane solution dataset (51 events), which includes all the Lucanian Apennines from the Irpinia-Potentino area, to the North, to the northwestern Pollino Range, to the South, gives a stress field with a sub-vertical  $\sigma_1$  and a sub-horizontal NE-directed  $\sigma_3$ . The relatively high average misfit value (7.9), however, indicates an inhomogeneous stress distribution within the studied region. These results suggest to perform new inversions in order to better analyze the stress heterogeneity within the selected area. Taking into account the scarcity of background seismicity in the Vallo di Diano and in the Upper Val d'Agri, we subdivided the main dataset in two sub-datasets, one to the north and the other to the south of this seismic gap area. Inversion results for the northern part, the Irpinia-Potentino area (32 fault-plane solutions), show a quite similar orientation of the principal stress axes as in the previous inversion. The average misfit is still quite large (7.4). By contrast, the inversion results obtained for the southern

part, with the Moliterno-North-western Pollino Range data (19 focal mechanisms), show an homogeneous stress field (average misfit 5.1) with a sub-horizontal  $\sigma_3$  NE-oriented. In order to resolve the heterogeneities within the northern sector, we further subdivided this area into two new datasets. The eastern sector (Potentino, 15 events) is characterized by hypocentral depth generally deeper than the western sector (Irpinia, 14 events). In these two new inversions we decided not to include three fault plane solutions of isolated events located to the north and north-west of the Irpinia area. By comparing the Irpinia and the Potentino inversion results we observe a small counter-clockwise rotation ( $12^\circ$ ) of the minimum compression stress axis ( $\sigma_3$ ) and a more oblique  $\sigma_1$  (plunge from  $71^\circ$  in Irpinia to  $58^\circ$  in Potentino). This difference in stress orientation and in misfit value (5.9 in Irpinia and 6.3 in Potentino) could be due to a high variability of stress in space between these two adjacent areas. Probably the Potentino area suffers the influence of the stress field change from the pure extension within the Apenninic chain to a transtension stress regime in the outer margin of the chain.

The generalized NE extension in this portion of the Southern Apennines could be explained by the buoyancy forces which are related to the westward subduction of the Adriatic continental lithosphere beneath the Apennines. Moreover, from tomographic images there is evidence of a less dense slab at depths shallower than 250 km (*Amato et al.*, 1993; *Lucente et al.*, 1999; *Cimini and De Gori*, 2001). Some studies interpret it as a detached slab in which the thermal assimilation of the subducted lithosphere brings to the consequent diminution of the forces acting on it (*Spakman*, 1990; *Spakman et al.*, 1993). More recently *De Gori et al.* (2001), through detailed tomographic studies focused on the Southern Apennines, have pointed out the presence of an almost continuous high-velocity body extended from 65 km down to 285 km of depth. They interpreted it as Adriatic lithosphere subducted beneath the Southern Apennines. This result can be explained considering that the previous tomography images had a poor resolution at shallow depths below the studied region. Another characteristic of the Southern Apennines subduction is the absence of a Benioff plane. *Carminati et al.* (2002) have suggested that the absence of seismicity at intermediate depth (60-300 km) could be related to the

continental composition of the subducted Adriatic lithosphere which is expected to have ductile rather than brittle behaviour.

The results coming from present-day stress field studies, as shown in this work, give important contributes to seismotectonic zoning and seismic hazard assessment. A detailed active stress map may tell us which faults are more likely to rupture in future events, and with which mechanism, specially in regions where active faults have no surface expression as in some part of Italy. In fact, many moderate but hazardous earthquakes occur on blind faults in the Italian region, with large repeat times of the order of thousands of years. For this reason it is important to integrate the stress field data with historical information and with seismicity patterns determined from instrumental monitoring in order to extend our possibility of assessing seismic hazard.

## **References**

- Amato, A., Alessandrini, B., Cimini, G.B., Frepoli, A., and Selvaggi G., 1993. Active and remnant subducted slabs beneath Italy: evidence from seismic tomography and seismicity. *Ann. Geofis.*, 36 (2), 201-214.
- Argus, D. F., Gordon, R.G., DeMets, C., and Stein, S., 1989. Closure of the Africa-Eurasia-North America Plate Motion Circuit and Tectonics of the Gloria Fault. *J. Geophys. Res.* 94, B5, 5585-5602.
- Azzara, R., Basili, A., Beranzoli, L., Chiarabba, C., Di Giovambattista, R., Selvaggi, G., 1993. The seismic sequence of Potenza (May 1990). *Ann. Geofis.*, 36 (1), 237-243.
- Barberi, G., Casentino, M.T., Gervasi, A., Guerra, I., Neri, G., Orecchio, B., 2004. Crustal seismic tomography in the Calabrian Arc region, South. Italy. *Phys. Earth Planet. Inter.* 147, 297-314.
- Boschi, E., Pantosti, D., Slejko, D., Stucchi, M., Valensise, G. (Editors), 1990. Irpinia dieci anni dopo. *Ann. Geofis.*, XXXVI (1), pp. 363.
- Carminati, E., Giardini, F., and Doglioni, C., 2002. Rheological control on subcrustal seismicity in the Apennines subduction (Italy). *Geophys. Res. Lett.*, 29(18), 1882, doi:10.1029/2001GL014084.
- Cassinis, R., Scarascia, S., Lozej, A., 2003. The deep crustal structure of Italy and surrounding areas from seismic refraction data. A new synthesis. *Boll. Soc. Geol. It.*, 122, 365-376.

- Castello, B., Selvaggi, G., Chiarabba, C., Amato, A., 2005. CSI Catalogo della sismicità italiana 1981-2002. Versione 1.0 (INGV-CNT, Roma), (on line: <http://www.ingv.it/CSI/>).
- Chatelain, J.L., 1978. Etude fine de la sismicité en zone de collision continentale à l'aide d'un réseau de stations portables: la region Hindu-Kush-Pamir . Thèse de 3<sup>ème</sup> cycle, Univ. Paul Sabatier, Toulouse.
- Chiarabba, C., and Amato, A., 1996. Crustal velocity structure of the Apennines (Italy) from P-wave travel time tomography. *Ann Geofis.*, XXXIX (6), 1133-1148.
- Chiarabba, C., Frepoli, A., 1997. Minimum 1D velocity models in Central and Southern Italy: a contribution to better constrain hypocentral determinations. *Ann. Geofis.*, XL (4), 937-954.
- Chiarabba, C., Jovane, L., Di Stefano, R., 2005. A new view of Italian seismicity using 20 years of instrumental recordings. *Tectonophysics*, 395, 251-268.
- Cimini, G.B., and De Gori, P., (2001). Nonlinear P-wave tomography of subducted lithosphere beneath central-southern Apennines (Italy), *Geophys. Res. Lett.*, 28 (23), 4387-4390.
- Cimini, G.B., De Gori, P., Frepoli, A., 2006. Passive seismology in Southern Italy: the SAPTEX array. *Ann. Geofis.*, 49 (2/3), 825-840.
- CPT Working Group, 1999. Catalogo Parametrico dei Forti terremoti Italiani (GNDT-ING-SGA-SSN). (Ed. Compositori, Bologna), pp.88.
- Cucci, L., Pondrelli, S., Frepoli, A., Mariucci M.T., and Moro M., 2004. Local pattern of stress field and seismogenic sources in the Pergola-Melandro Basin and the Agri Valley (Southern Italy). *Geophys. J. Int.*, 156 (3), 575-583.
- De Gori, P., Cimini, G.B., Chiarabba, C., De Natale, G., Troie, C., and Deschamps, A., 2001. Teleseismic tomography of the Campanian volcanic area and surrounding Apenninic belt. *J. Volcanol. Geotherm. Res.*, 109, 55-75.
- De Mets, C., Gordon, R.G., Argus, D.F., Stein, S., 1990. Current plate motions. *Geophys. J. Int.* 104, 73-74.
- Di Luccio, F., Fukuyama, E., Pino, N.A., 2005. The 2002 Molise earthquake sequence: What can we learn about the tectonics of Southern Italy? *Tectonophysics*, 405, 141-154.



- Ekstrom, G., 1994. Teleseismic analysis of the 1990 and 1991 earthquakes near Potenza. *Ann. Geofis.*, 37 (6), 1591-1599.
- Frepoli, A., and Amato A., 2000. Fault plane solutions of crustal earthquakes in Southern Italy (1988-1995): seismotectonic implications. *Ann. Geofis.*, 43 (3), 437-467.
- Frepoli, A., Cinti, F.R., Amicucci, L., Cimini, G.B., De Gori, P., Pierdominici, S., 2005. Pattern of seismicity in the Lucanian Apennines and foredeep (Southern Italy) from recording by SAPTEX temporary array. *Ann. Geofis.*, 48 (6), 1035-1054.
- Gentile, G. F., Bressan, G., Burlini, L., and De Franco R., 2000. Three-dimensional Vp and Vp/Vs models of the upper crust in the Friuli area (northeastern Italy). *Geophys. J. Int.*, 141,457-478.
- Gephart, J.W. & Forsyth, D.W., 1984. An improved method for determining the regional stress tensor using earthquake focal mechanism data: application to the San Fernando earthquake sequence, *J. Geophys. Res.*, 89 (B11), 9305-9320.
- Gephart, J.W. (1990). FMSI: a Fortran program for inverting fault/slickenside and earthquake focal mechanism data to obtain the regional stress tensor, *Comput. Geosci.*, 16, 953-989.
- Harabaglia, P., Monelli F., and Zito, G., 1997. Geothermics of the Apennines subduction. *Ann. Geofis.*, XL (5), 1261-1274.
- Kissling, E., Ellsworth, W.L., Eberhart-Phillips, D., Kradolfer, U., 1995. Initial reference models in local earthquake tomography. *J. Geophys. Res.*, 99, 19635-19646.
- Lahr, J.C., 1989. HYPOELLIPSE/Version 2.0: a computer program for determining local earthquake hypocentral parameters, magnitude, and first motion pattern. *U. S. Geol. Surv. Open File Rep.*, 95, 89-116.
- Locardi, E., and Nicolich, R. (1988). Geodinamica del Tirreno e dell'appennino centromeridionale, la nuova carta della Moho. *Mem. Soc. Geol. It.*, 41, 121-140.
- Lucente, F.P., Chiarabba, C., Cimini, G.B., and Giardini, D., 1999. Tomographic constraints on the geodynamic evolution of the Italian region. *J. Geophys. Res.*, 104(B9), 20,307-20,328.

- Malinverno, A., and Ryan, W.B.F, 1986. Extension in the Tyrrhenina Sea and shortening in the Apennines as result of arc migration driven by sinking of the lithosphere. *Tectonics*, 5, 227-245.
- Maschio, Ferranti, L., and Burrato, P., 2005. Active extension in Val d'Agri area, southern Apennines, Italy: implications for the geometry of the seismogenic belt. *Geophys. J. Int.*, 162, 591-609.
- Meletti, C., Valensise, G., Azzaro, R., Barba, S., Basili, R., Galadini, F., Gasperini, P., Stucchi, M., Vanucci, G., 2004. Zonazione sismogenetica ZS9-App.2 al rapporto conclusivo.(on line: <http://zonesismiche.mi.ingv.it/documenti/App2.pdf>)
- Merlini, S., Cippitelli, G., 2001. Structural styles inferred by seismic profiles, in *Anatomy of an Orogen: the Apennines and adjacent Mediterranean Basins*. G.B. Vai and I.P. Martini (eds.), Kluwer Academic Publishers, 441-454.
- Michetti, A.M., Ferrelli, L., Esposito, E., Porfido, E., Blumetti, A.M., Vittori, E., Serva, L., and Roberts, G.P, 2000. Ground effects during the 9 september 1998, Mw = 5.6, Lauria earthquake and the seismic potential of the "aseismic" Pollino region in Southern Italy. *Seimological Research Letters*, 41 (1), 31-46.
- Montone, P., Mariucci, M.T., Pondrelli S., and Amato, A., 2004. An improved stress map for Italy and surrounding regions (Central Mediterranean). *J. Geophys. Res.*, 109.
- Morelli, C. (2000). The themes of crustal research in Italy and the role of DSS-WA seismics, *Boll. Soc. Geol. It.*, 119, 141-148.
- Pointoise, B., Monfret, T., 2004. Shallow seismogenic zone detected from an offshore-onshore temporary seismic network in the Esmeraldas area (Northern Ecuador). *Geochem. Geophys. Geosyst.*, 5 (2), 1-22.
- Pondrelli, S., Morelli, A., Ekström, G., Mazza, S., Boschi E., and Dziewonski, A.M., 2002. European-Mediterranean regional centroid-moment tensor:1997-2000. *Phys. Earth Planet. Int.*, 130, 71-101.
- Reasenberg, P., and Oppenheimer, D., 1985. FPFIT, FPLOT and FPPAGE: FORTRAN computer programs for calculating and displaying earthquake fault-plane solutions. U.S. Geol. Surv. Open-File Rep. 85-739.

Scrocca, D., Carminati, E., Doglioni, C., 2005. Deep structure of southern Apennines, Italy: Thin-skinned or thick-skinned? *Tectonics*, 24, 1-20.

Spakman, W., 1990. Tomography images of the upper mantle below central Europe and the Mediterranean. *Terra Nova*, 2, 542-553.

Spakman, W., Van der Lee, S., and Van der Hilst, R., 1993. Travel-time tomography of the European-Mediterranean mantle down to 1400 km. *Phys. Earth Planet. Inter.*, 79, 3-74.

Tiberti, M.M., Orlando, L., Bucci, D., Bernarbini, M., Parotto, M., 2005. Regional gravity anomaly map and crustal model of the Central-Southern Apennines (Italy). *Journal of Geodynamics*, 40, 73-91.

Ventura, G., Cinti, F.R., Di Luccio, F., Pino, N.A., 2007. Mantle wedge dynamics vs crustal seismicity in the Apennines (Italy). *Geochem. Geophys. Geosyst.*, 8 (2), 1525-2027.

Wyss M., Liang B., Tanigawa, W.R., and Wu, X., 1992. Comparison of orientations of stress and strain tensors based on fault-plane solutions in Kaoiki, Hawaii, *J. Geophys. Res.*, 97, 4769-4790.

**Table I:** Weights assigned to each P- and S- arrival time on the basis of picking accuracy.

<b>Weights</b>	<b>Picking accuracy (s)</b>
1	0,04
2	0,10
3	0,20
4	0,40

**Table II:** Quality based on the value of the horizontal error SEH (68% confidence limit), and vertical error SEZ (68% confidence limit).

<b>Quality</b>	<b>Larger of SEH and SEZ</b>	<b>Model Test_8</b>		<b>Model Vel_8</b>	
		<b>Number of events</b>	<b>% number of events</b>	<b>Number of events</b>	<b>% number of events</b>
A	$\leq 1.34$	243	67,7%	173	56,90%
B	$\leq 2.67$	59	16,40%	70	23,10%
C	$\leq 5.35$	25	7,00%	36	11,80%
D	$> 5.35$	32	8,90%	25	8,20%

**Table III:** Velocity values of the best model for Lucanian Apennines computed with VELEST code.

Top of layer (km)	Velocity of model Test8 (km/s)
0	5,25
-5	5,92
-17	6,28
-35	7,14
-45	7,49
-50	8,1

**Table IV:** Value of quality factor  $Q_f$  and  $Q_p$  for Fault-plane solution.  $F_j = 0$  indicate a perfect fit to the data, while  $F_j = 1$  is a perfect misfit.  $\Delta s$ ,  $\Delta d$  and  $\Delta r$  are ranges of perturbation of strike, dip and rake, respectively.

Quality	$Q_f$	$Q_p$
A	$F_j \leq 0.025$	$\Delta s, \Delta d, \Delta r \leq 20^\circ$
B	$0.025 < F_j \leq 0.1$	$20^\circ$ to $40^\circ$
C	$F_j > 0.1$	$> 40^\circ$

**Table V.** Selected Southern Italy fault plane solutions selected. Date in format year-month-day; O.T = origin time (hour and minute); Latitude North and Longitude east; Depth in km; MI = local magnitude of events belonging to the 2001-2002 period from the Italian Seismic Catalogue (CSI) and of 2003-2004 period from INGV Seismic Bulletin; r.m.s.= root mean square of residuals of re-location; ERH and ERZ = horizontal and vertical location errors; strike, dip and rake of the first nodal plane;  $Q_f$  and  $Q_p$ ,= focal mechanism quality factors based on misfit and confidence regions; N. P.= polarities number; category = fault plane solution type (SS = strike-slip, NS = normal fault with small strike-slip component, TS = thrust fault with small strike-slip component, NF = normal fault, TF = thrust fault, U = undefined solution category); area = geographical locality of event epicenter.

No	Date	O.T.	Latitude	Longitude	Depth	MI	Rms	ERH	ERZ	strike	dip	Rake	$Q_f$	$Q_p$	N. P.	category	Area
----	------	------	----------	-----------	-------	----	-----	-----	-----	--------	-----	------	-------	-------	-------	----------	------

1	010914	08:02	40° 37.68	15° 44.01	18.88	2.4	0.39	0.5	0.1	140	35	-120	B	A	11	NF	Potentino
2	011104	10:22	40° 25.78	16° 05.41	11.75	2.1	0.55	0.5	0.0	140	70	-60	A	A	10	NF	Dolomiti Lucane
3	011113	13:21	40° 31.55	15° 56.28	34.73	1.9	0.73	0.5	0.1	130	65	150	A	A	13	SS	Potentino
4	011121	06:10	40° 32.27	15° 49.28	2.34	2.5	0.93	0.3	0.1	115	80	-80	B	B	13	NF	Potentino
5	011121	06:21	40° 31.66	15° 49.86	12.26	2.3	0.22	0.7	0.0	165	75	-50	B	A	12	NS	Potentino
6	011209	12:15	40° 47.62	15° 17.14	11.75	3.3	0.45	0.4	0.1	70	50	-160	B	A	15	NS	Irpinia
7	020115	00:06	40° 46.70	15° 48.24	14.24	2.1	0.32	0.7	0.9	140	40	-90	A	B	8	NF	Potentino
8	020208	04:38	40° 14.99	15° 55.72	11.22	2.2	0.14	0.4	0.1	60	65	-170	B	A	11	SS	Moliterno
9	020226	17:12	40° 14.41	15° 55.46	4.07	2.1	0.32	0.3	0.1	20	65	-20	A	A	8	SS	Moliterno
10	020317	04:53	40° 14.98	15° 55.91	11.15	2.6	0.16	0.5	0.1	60	65	-180	B	B	10	SS	Moliterno
11	020324	00:11	40° 16.98	16° 34.81	47.48	2.4	0.59	0.7	0.1	190	40	-100	A	A	11	NF	Policoro-Montalbano Jonico
12	020328	09:59	40° 19.14	17° 23.36	39.98	2.6	0.95	1.1	1.3	325	90	-170	B	B	18	SS	Murge Tarantine
13	020413	08:44	40° 30.11	15° 50.18	11.41	2.4	0.37	0.4	0.1	115	70	-180	A	A	12	SS	Potentino
14	020413	10:48	40° 11.56	15° 55.20	12.13	2.1	0.20	0.6	0.1	285	80	-140	A	B	8	SS	Moliterno
15	020413	17:04	40° 34.09	16° 24.78	21.68	3.0	0.38	0.3	0.1	340	35	-120	B	A	31	NF	Basentano
16	020413	20:28	40° 33.39	16° 25.71	22.90	2.1	0.20	0.8	0.1	10	10	-50	A	B	8	NS	Basentano
17	020418	21:00	40° 35.22	15° 34.55	10.51	3.0	0.31	0.5	0.0	200	80	-10	A	B	17	SS	Savoia di Lucania
18	020418	21:36	40° 35.13	15° 34.77	9.96	2.2	0.28	0.5	0.0	200	85	-20	A	A	13	SS	Savoia di Lucania
19	020418	22:58	40° 34.96	15° 34.59	8.46	2.7	0.34	0.5	0.1	195	85	-10	A	B	12	SS	Savoia di Lucania
20	020419	18:06	40° 35.92	15° 34.51	4.46	2.5	0.25	0.8	0.3	170	45	-50	A	A	10	NF	Savoia di Lucania
21	020419	22:12	40° 35.30	15° 33.45	10.78	2.2	0.24	0.8	0.1	140	50	-20	A	A	10	NS	Savoia di Lucania
22	020429	03:19	40° 34.78	15° 33.65	11.62	2.8	0.20	0.6	0.1	25	55	-30	A	A	9	NS	Savoia di Lucania
23	020504	09:41	40° 39.56	15° 32.45	13.96	2.3	0.37	0.4	0.1	150	40	-60	A	A	10	NF	Irpinia
24	020505	06:40	40° 37.45	15° 37.93	20.01	1.9	0.23	0.6	0.1	65	45	-130	A	A	8	NF	Irpinia
25	020508	19:29	40° 05.47	15° 59.77	11.20	2.9	0.36	0.4	0.1	45	80	0	B	A	18	SS	Northern Pollino
26	020509	23:55	40° 23.64	16° 34.19	28.51	2.1	0.40	0.4	0.1	335	65	-120	B	A	12	NF	Basentano
27	020512	20:20	40° 37.73	15° 45.95	17.53	2.1	0.29	0.4	0.1	20	80	20	A	A	12	SS	Potentino
28	020531	16:31	40° 14.99	15° 55.00	9.88	2.5	0.24	0.5	0.1	140	70	-40	B	A	13	NS	Moliterno
29	020607	05:47	39° 59.72	16° 02.23	88.17	2.2	0.43	1.2	0.3	275	70	0	A	A	10	SS	Calabrian subduction zone
30	020611	20:02	40° 30.63	15° 43.49	13.08	2.1	0.50	0.3	0.1	125	65	-110	B	A	18	NF	Potentino
31	020618	23:31	40° 31.81	15° 45.87	9.92	2.3	0.43	0.3	0.0	345	80	-160	A	A	18	SS	Potentino
32	020621	19:34	40° 05.46	15° 58.99	7.40	2.4	0.52	0.4	0.1	155	65	-70	B	A	14	NF	Northern Pollino
33	020713	05:57	39° 59.52	16° 03.35	10.10	2.1	0.47	0.3	0.1	140	25	-60	B	A	11	NF	Northern Pollino
34	020713	11:49	39° 58.86	16° 04.97	10.44	2.7	0.30	0.8	0.1	105	35	-110	A	A	8	NF	Northern Pollino
35	020718	08:28	40° 00.28	16° 03.63	9.52	2.5	0.48	0.4	0.1	95	45	-120	A	A	9	NF	Northern Pollino
36	020815	12:58	39° 43.92	15° 57.69	31.05	2.1	0.56	0.9	0.0	40	85	-180	A	A	12	SS	Orsomarso
37	020903	01:45	40° 29.89	15° 41.34	13.38	1.9	0.36	0.4	0.1	70	60	-150	B	A	14	NS	Potentino
38	021004	22:58	40° 15.21	15° 55.58	9.86	2.9	0.35	0.4	0.1	230	85	180	A	A	17	SS	Moliterno
39	021006	02:43	40° 14.41	15° 55.16	9.76	1.9	0.22	0.5	0.1	80	90	-170	B	A	11	SS	Moliterno
40	021017	15:19	40° 24.87	15° 47.16	14.03	2.1	0.19	0.5	0.1	65	15	-50	B	B	11	NF	Upper Val d'Agri
41	021109	01:53	40° 49.76	15° 51.06	11.86	2.0	0.28	0.6	0.1	115	50	-90	A	A	8	NF	Potentino
42	021119	16:53	40° 14.27	15° 54.98	8.44	1.8	0.20	0.5	0.1	50	80	0	A	A	10	SS	Moliterno
43	021129	10:54	40° 14.14	15° 54.97	9.49	1.9	0.24	0.6	0.1	40	70	0	A	A	9	SS	Moliterno
44	021130	01:19	40° 14.19	15° 54.87	10.15	2.4	0.23	0.4	0.1	135	50	-70	A	A	13	NF	Moliterno
45	021130	17:33	40° 13.94	15° 55.00	11.06	2.2	0.18	0.4	0.1	5	70	30	B	A	13	SS	Moliterno
46	021201	00:30	40° 13.26	15° 55.48	5.23	2.1	0.31	0.3	0.1	160	25	-60	A	B	10	NF	Moliterno
47	021208	23:53	41° 15.43	16° 11.13	3.00	2.4	0.38	0.4	0.3	20	50	30	A	B	10	TS	Murge
48	030113	23:01	40° 15.30	15° 55.34	8.57	2.9	0.37	0.4	0.1	165	85	-70	A	A	8	U	Moliterno
49	030311	00:22	40° 53.64	16° 34.71	28.61	2.9	0.44	0.6	0.1	135	75	-110	A	A	15	NF	Murge
50	031118	06:08	39° 10.19	16° 28.56	12.92	3.5	0.32	0.6	0.3	110	55	-80	A	B	12	NF	Sila

51	040223	19:48	40°	43.03	15°	26.23	13.32	3.6	0.39	0.5	0.1	180	50	-80	A	A	13	NF	Irpinia
52	040903	00:04	40°	41.66	15°	40.16	11.67	4.1	0.59	0.3	0.0	120	35	-120	B	A	25	NF	Potentino
53	040903	01:22	40°	41.46	15°	40.31	11.34	2.8	0.25	0.4	0.1	160	45	-80	A	A	10	NF	Potentino
54	041126	01:49	41°	03.13	15°	28.31	6.58	3.0	0.35	0.4	0.1	200	75	-40	A	A	9	SS	Northern Irpinia
55	050521	19:55	41°	02.21	14°	32.52	4.87	3.7	0.67	0.4	0.1	35	65	-30	A	A	11	SS	Cervinara
56	050927	22:33	38°	38.42	17°	06.78	17.05	3.7	0.85	0.8	0.1	345	10	-100	A	A	9	NF	Ionian Sea
57	051111	00:41	40°	53.15	15°	49.02	11.12	2.4	0.31	0.4	0.1	75	90	-140	A	A	8	U	Potentino
58	051118	18:35	39°	07.04	17°	11.75	8.15	3.5	0.41	1.0	0.2	40	45	-170	B	A	11	U	Crotone
59	060717	16:56	40°	46.69	15°	29.65	6.44	2.5	0.36	0.3	0.1	125	45	-90	A	B	9	NF	Irpinia
60	060907	15:31	40°	34.93	16°	9.59	25.24	3.9	0.35	0.3	0.1	75	10	-110	B	A	22	U	Basentano
61	060915	17:55	40°	46.09	15°	22.34	12.52	2.4	0.28	0.4	0.1	150	65	-20	A	A	11	SS	Irpinia
62	060926	16:29	40°	43.29	15°	27.91	4.80	3.0	0.39	0.3	0.1	110	75	-100	A	A	15	NF	Irpinia
63	061022	00:38	40°	04.92	15°	53.15	13.02	2.4	0.33	0.5	0.1	15	50	-80	A	A	9	NF	Northern Pollino
64	061201	15:38	40°	46.58	15°	26.96	13.24	2.7	0.30	0.4	0.1	150	30	-100	A	A	12	NF	Irpinia
65	061205	06:20	41°	05.62	15°	16.79	13.35	2.5	0.46	0.4	0.1	160	65	-100	B	A	10	NF	Northern Irpinia

## Figures Captions

**Fig.1.** Seismicity of Southern Italy from 1981 to 2005 (CPTI Working Group, 1999; Castello *et al.*, 2005). Historical earthquakes are shown with the year of occurrence close to unfilled red squares with size proportional to the estimated magnitude. Focal mechanisms of the largest events in the Southern Apennines in the last 27 years are also shown (Irpinia 1980, Potentino area 1990 and 1991, Castelluccio area 1998).

**Fig.2.** Italian National Seismic Network (RSNC) and SAPTEX temporary seismic stations used in the study . White squares show the permanent stations of the RSNC and circles show the temporary stations deployed for the SAPTEX tomographic experiment during 2001 (orange), 2002 (blue), 2003 (magenta), and 2004 (green) (Cimini *et al.*, 2006).

**Fig.3.** Linear fit of DTs versus DTp within 95% prediction bounds using Linear Least Squares Method with a Matlab code. The root mean squared error (RMSE) is 0.40, and the linear correlation coefficient (R) is 0.87.

**Fig.4.** Starting P-wave velocity model for the Italian region computed by Chiarabba *et al.* (2005). We re-stratified this initial model introducing some layers with thickness of 3 or 4 km, up to 30 km depth, and of 5 km for greater depths. We named this model *Model2*. *Vel\_8* is the final velocity model obtained with VELEST.

**Fig.5.** Hypocentral distribution versus depth for the model *Vel\_8*.

**Fig.6.** Starting P-wave velocity model for the Southern Italy by Chiarabba and Frepoli (1997). We re-stratified this starting model introducing some layers with thickness of 3 or 4 km, up to 30 km depth, and of 5 km for greater depth. We named this model *Modell*. *Vel\_9* is the final velocity model obtained with VELEST.

**Fig.7.** Hypocentral distribution versus depth for the model *Vel\_9*.

**Fig.8.** Starting P-wave velocity model *Test* for the Lucanian Apennines. We re-stratified this model introducing some layers with thickness of 3 or 4 km, up to 30 km depth, and of 5 km for greater depths. We named this model *Teststra*. *Test8* is the final velocity model obtained with VELEST.

**Fig.9.** Hypocentral distribution versus depth for the model *Test8*.

**Fig.10.** P-wave velocity final models obtained by VELEST. *Vel\_8* is the model derived from *Model2*, *Vel\_9* from *Modell* and *Test8* from *Teststra*.

**Fig.11.** Epicentral distribution of the 359 earthquakes located using the model *Test8*. The width of cross-sections AB, CD, EF, GH, and IL is 25 km. The width of profile MN is 200 km.

**Fig.12.** Depth distribution of 359 events located with HYPOELLIPSE using the model *Test8*.

**Fig.13.** Location and error ellipse (99% confidence limit) of events with quality A, B and C.

**Fig.14.** Distribution of: a) RMS values; b) maximum horizontal error (Err\_H); c) distribution of vertical error (Err\_Z) for events relocation. In b) and c) we considered only events with horizontal and vertical errors less than 10 km.

**Fig.15a,b.** Distribution of the 65 selected fault-plane solutions. Event numbers of Table V are shown close to each focal mechanism. Coloured lines encircle the crustal volume considered for the stress inversion: blue line for the inversion with 51 fault-plane solutions; green lines for the two inversions of the Irpinia-Potentino area to the North (32 events) and the Moliterno-Northwestern Pollino area to the South (19 events); yellow lines for the two inversions of the adjacent areas of Irpinia (14 focal mechanisms) and Potentino (15 events).

**Fig.16.** Stress inversion results using: a) 51 solutions (Apenninic chain); b) 32 solutions (Irpinia-Potentino); c) 19 solutions (Moliterno-Pollino); d) 14 solutions (Irpinia); e) 15 solutions (Potentino). For each inversion is shown the stereonet plot with the 95% confidence limits for  $\sigma_1$  (small crosses) and  $\sigma_3$  (small squares) and the histogram illustrating the uncertainty in the R parameter. Plunge and trend for the three principal stress axes are shown below the histograms.



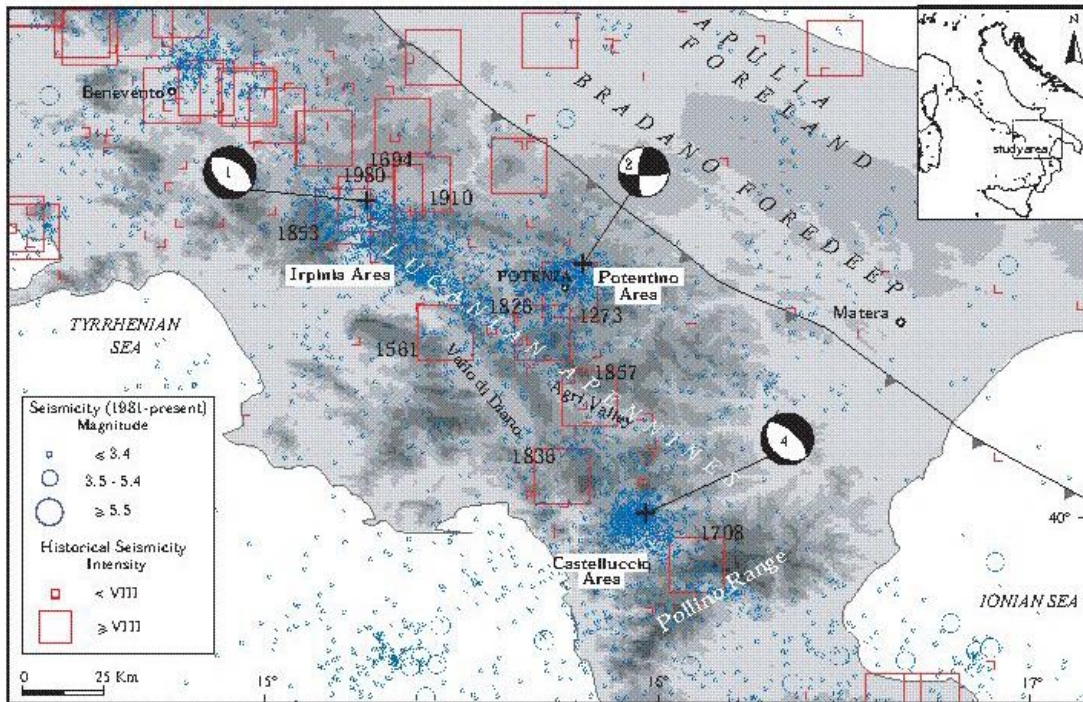


Fig.1

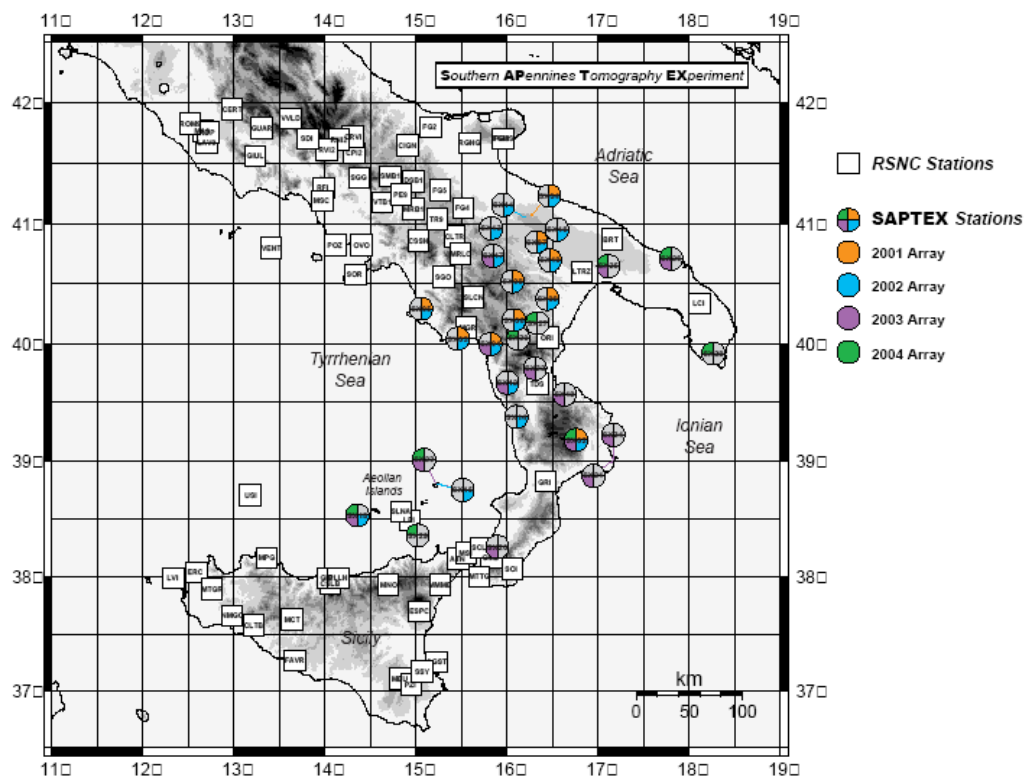


Fig.2

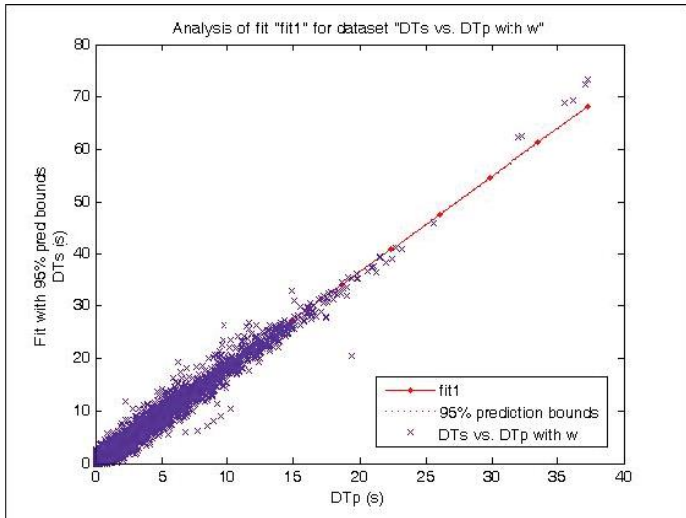


Fig.3

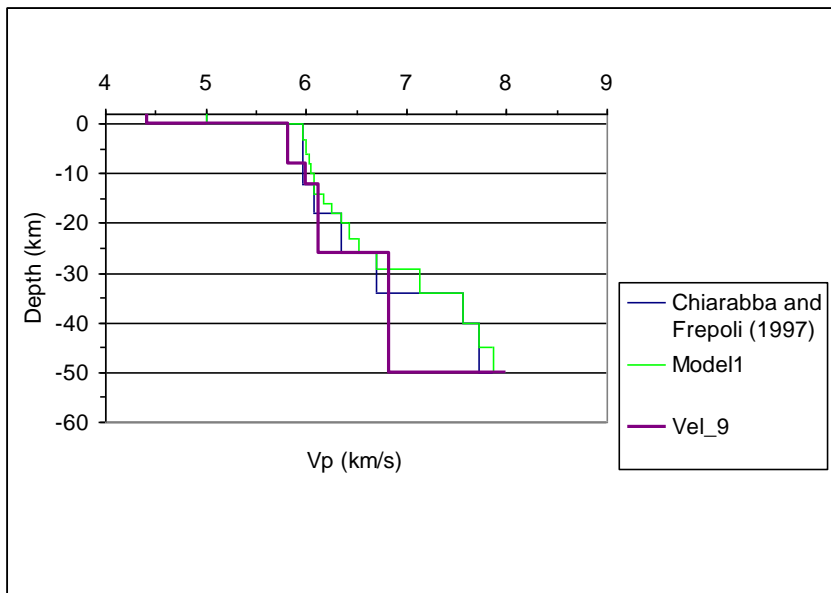


Fig.4

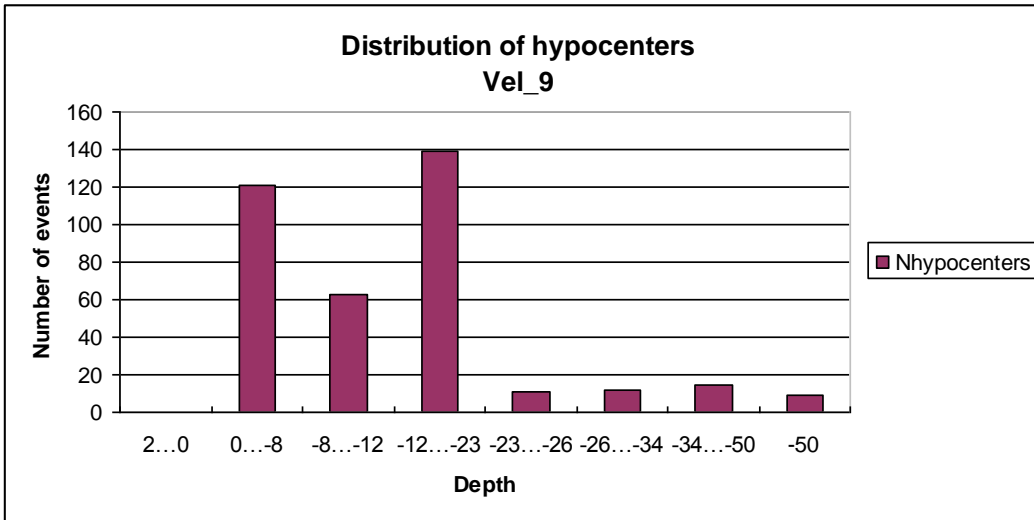


Fig.5

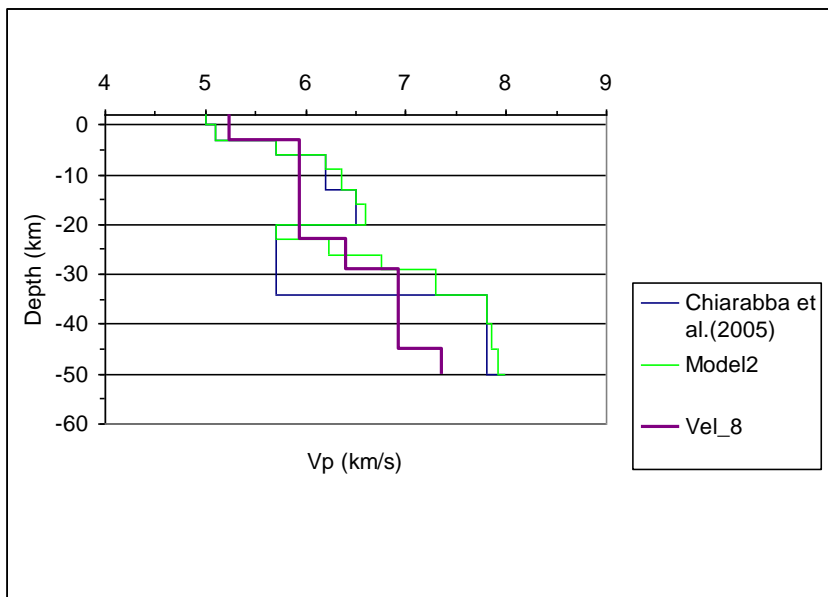


Fig.6

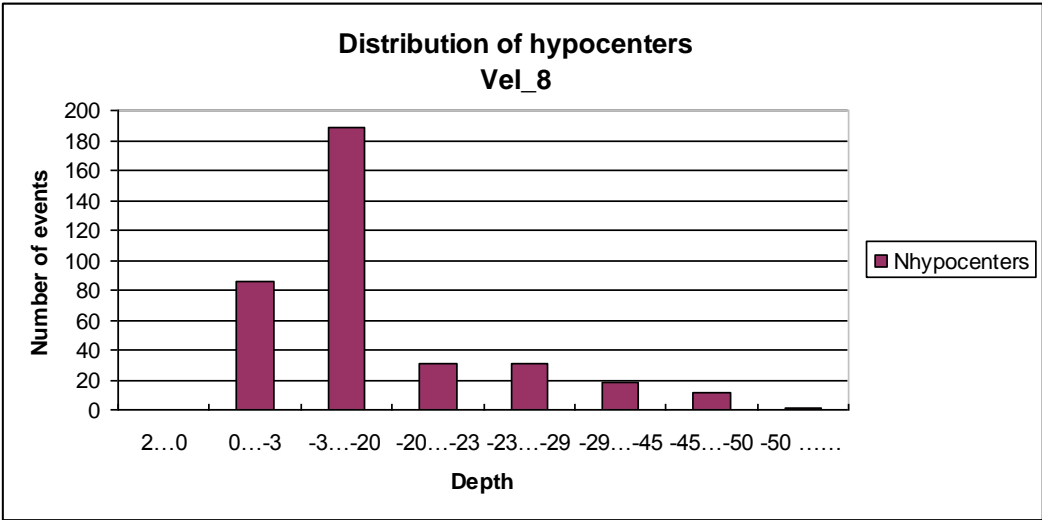


Fig.7

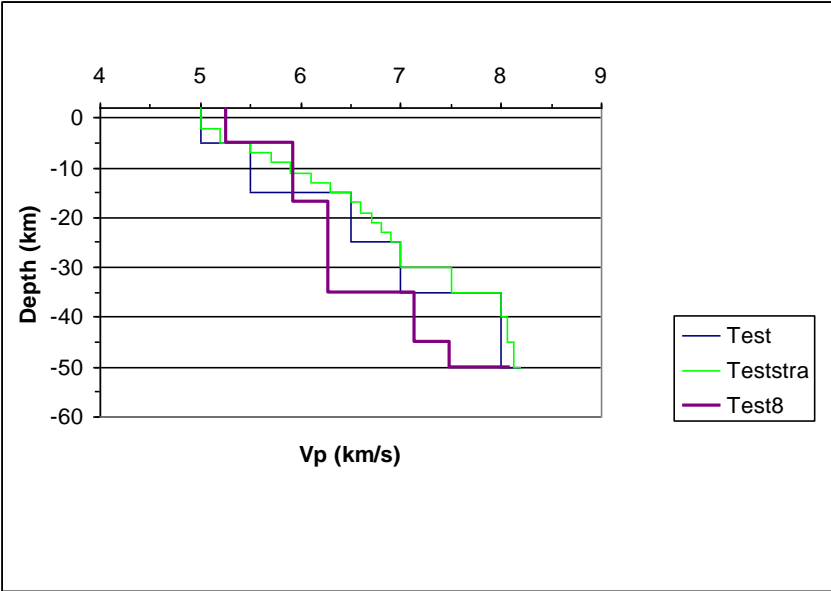


Fig.8

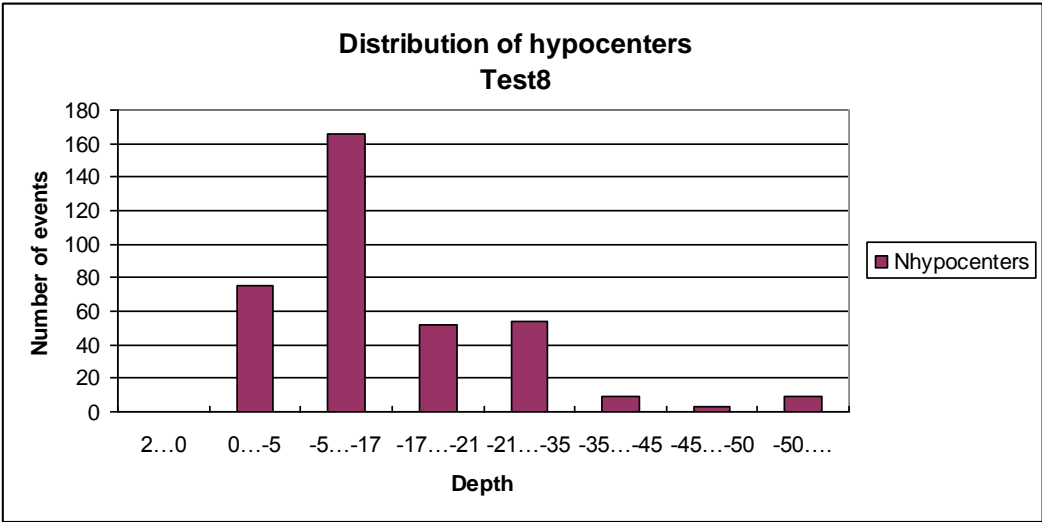


Fig.9

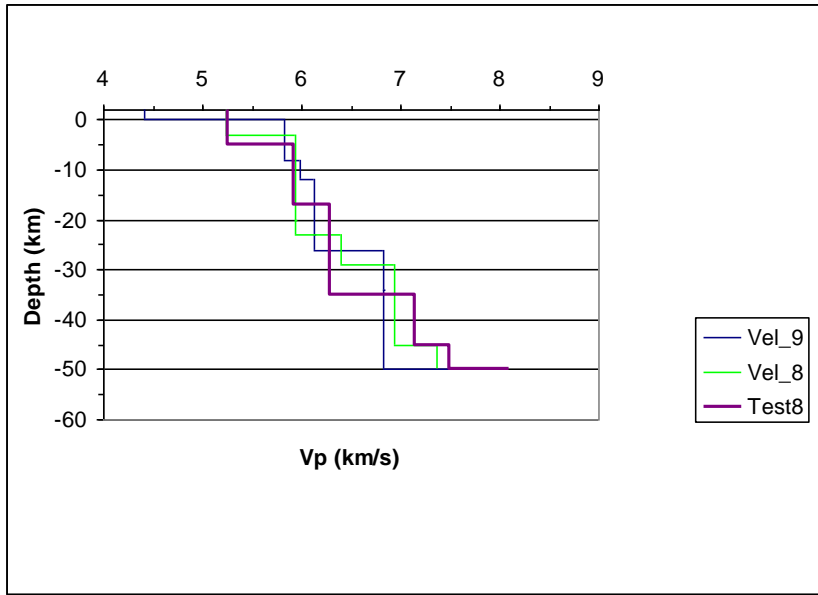


Fig.10

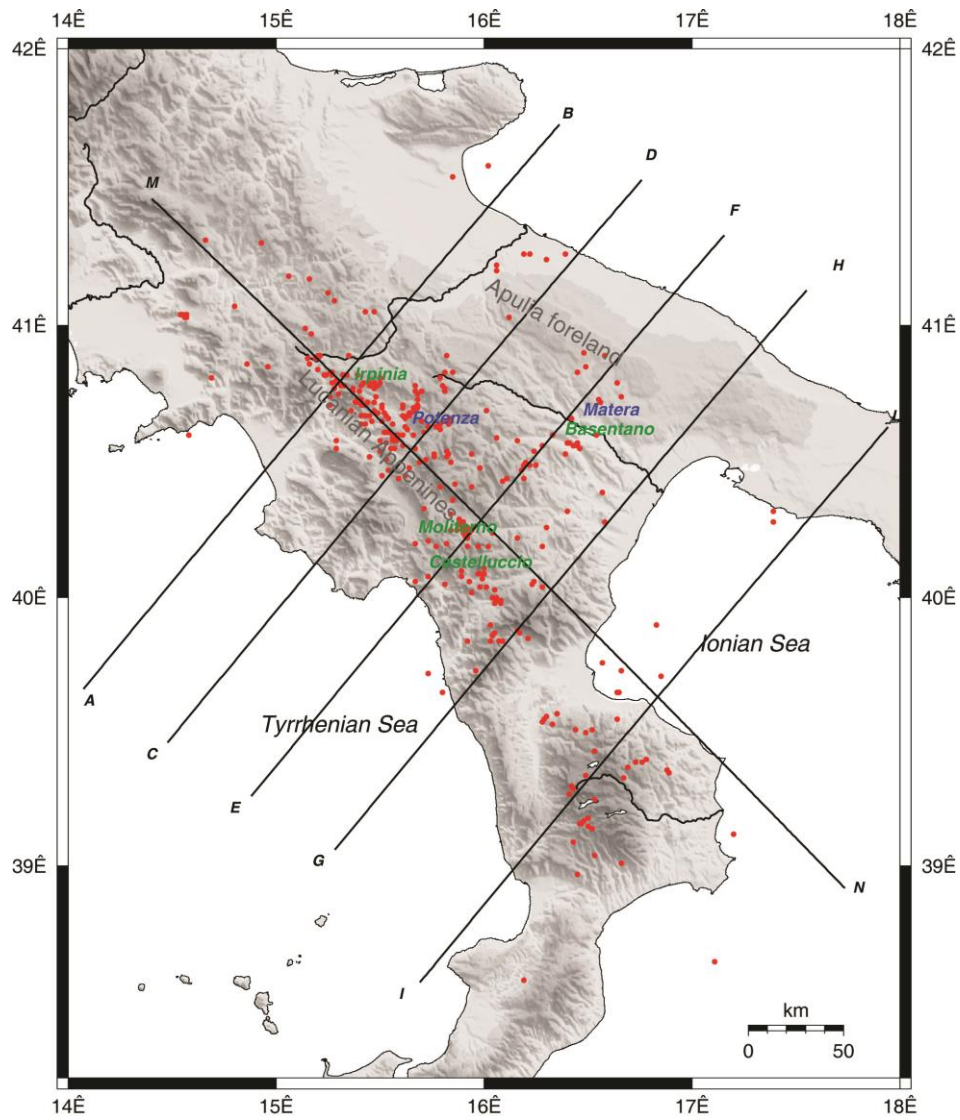


Fig.11

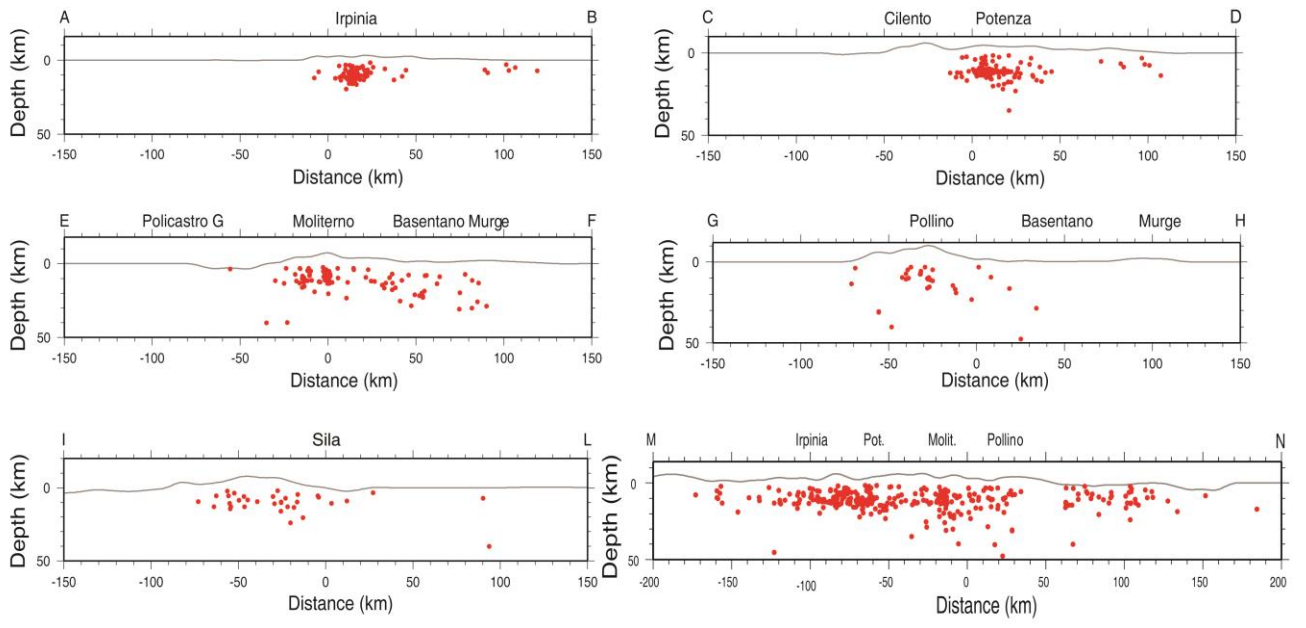


Fig.12

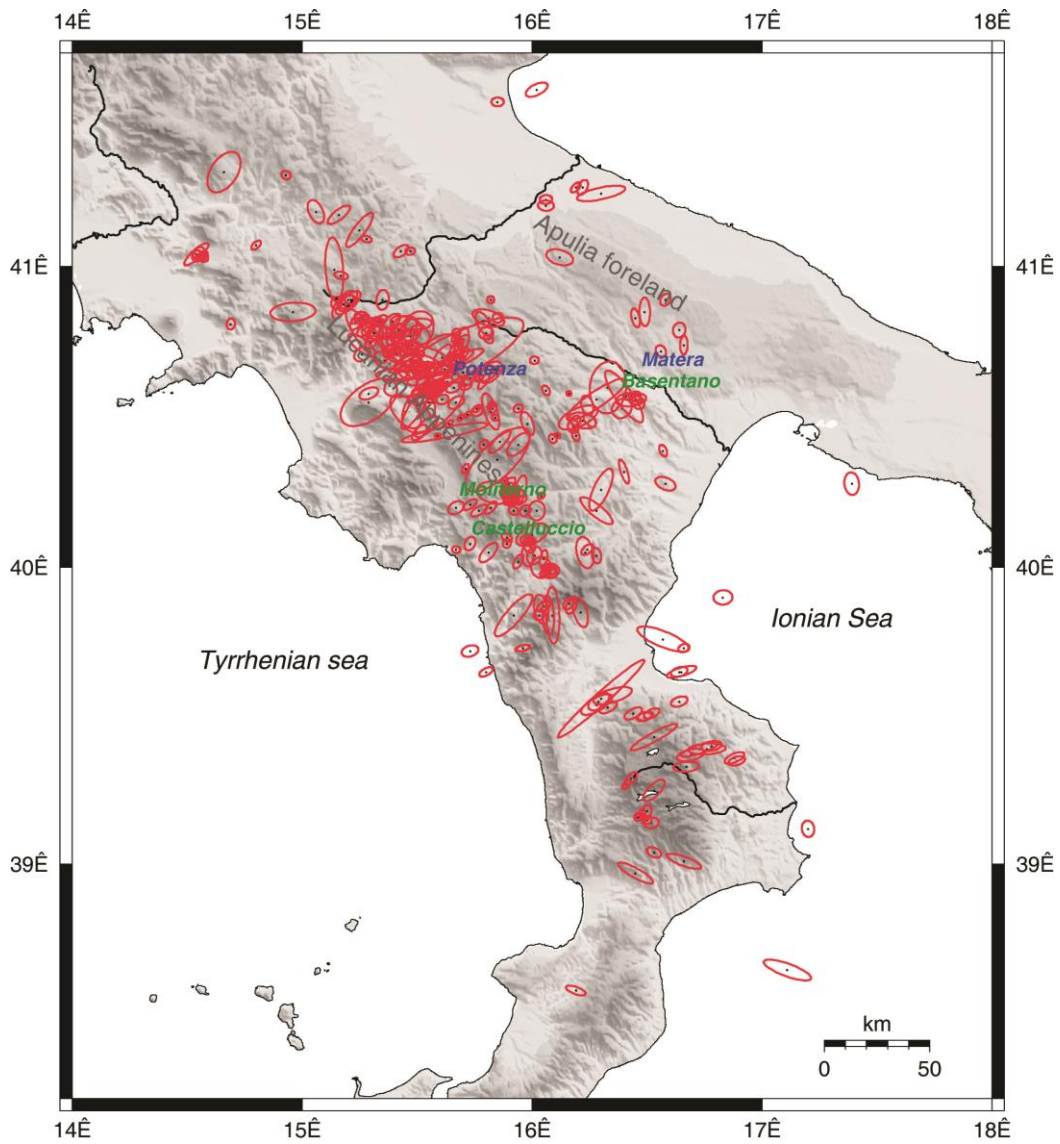


Fig.13

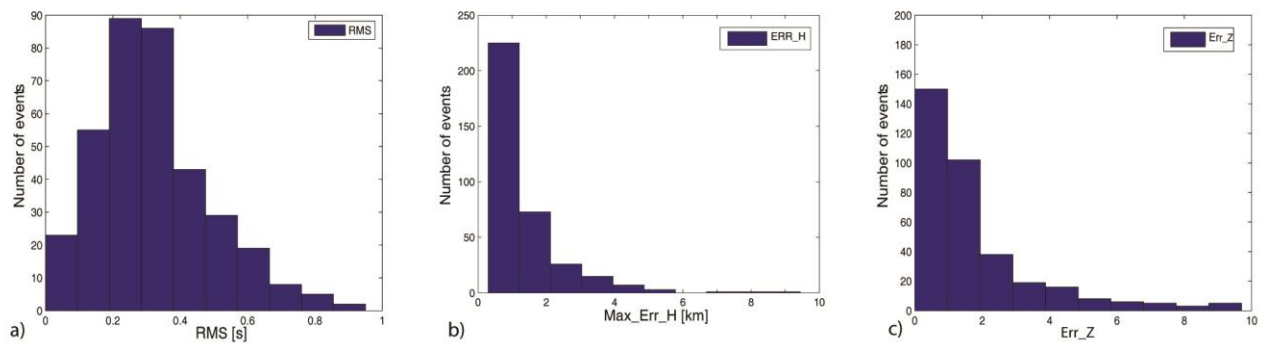


Fig.14



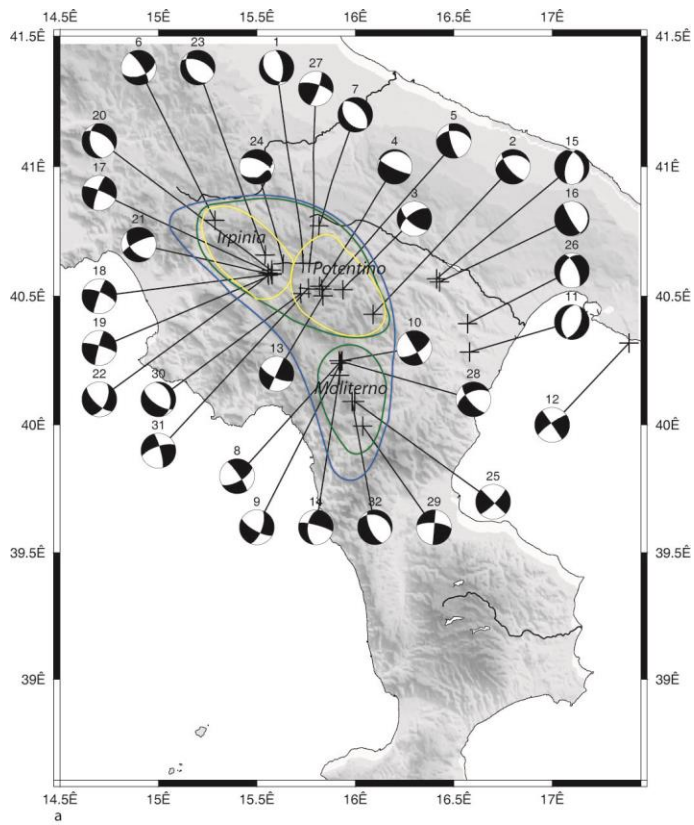


Fig.15a

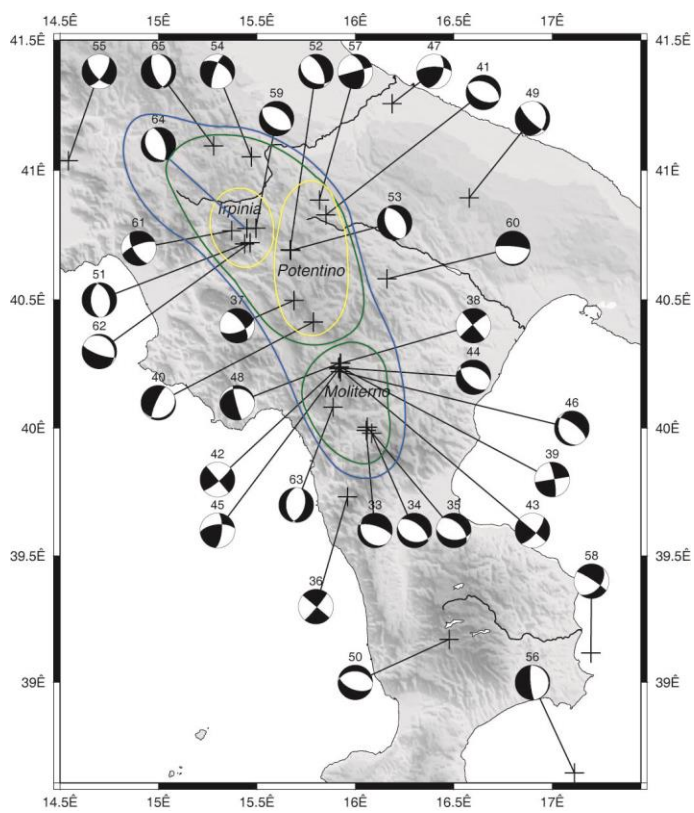


Fig.15b

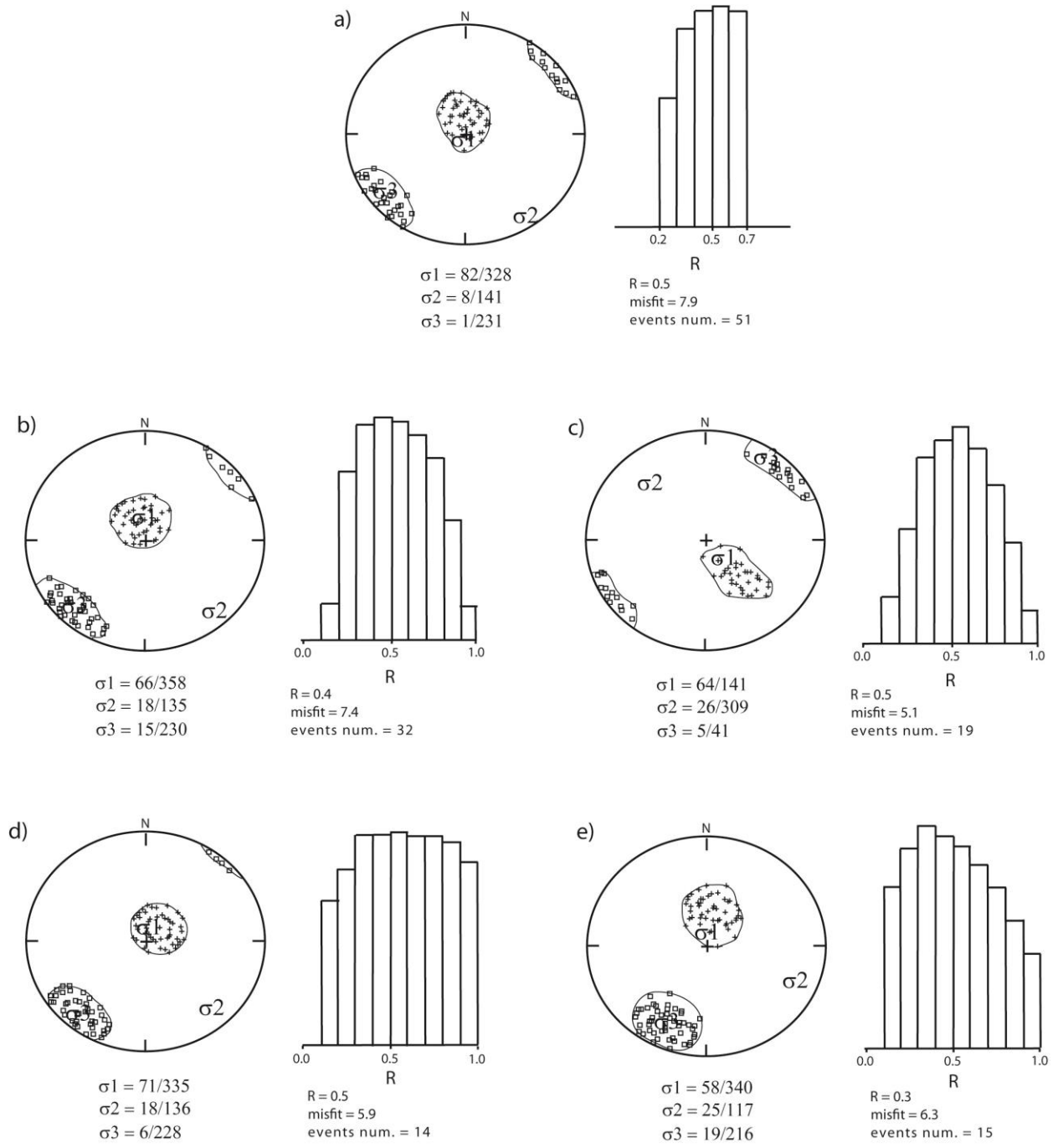


Fig.16